SCIENTIFIC REPORTS

OPEN

Zeolite Nanoparticles for Selective Sorption of Plasma Proteins

M. Rahimi[1,*], E.-P. Ng[2,*], K. Bakhtiari[3,4], M. Vinciguerra[5], H. Ali Ahmad[6], H. Awala[6], S. Mintova[6], M. Daghighi[7], F. Bakhshandeh Rostami[8], M. de Vries[9], M. M. Motazacker[10], M. P. Peppelenbosch[11,*], M. Mahmoudi[12,13,*] & F. Rezaee[9,11]

Received: 23 July 2015
Accepted: 23 October 2015
Published: 30 November 2015

The affinity of zeolite nanoparticles (diameter of 8–12 nm) possessing high surface area and high pore volume towards human plasma proteins has been investigated. The protein composition (corona) of zeolite nanoparticles has been shown to be more dependent on the plasma protein concentrations and the type of zeolites than zeolite nanoparticles concentration. The number of proteins present in the corona of zeolite nanoparticles at 100% plasma (*in vivo* state) is less than with 10% plasma exposure. This could be due to a competition between the proteins to occupy the corona of the zeolite nanoparticles. Moreover, a high selective adsorption for apolipoprotein C-III (APOC-III) and fibrinogen on the zeolite nanoparticles at high plasma concentration (100%) was observed. While the zeolite nanoparticles exposed to low plasma concentration (10%) exhibited a high selective adsorption for immunoglobulin gamma (i.e. IGHG1, IGHG2 and IGHG4) proteins. The zeolite nanoparticles can potentially be used for selectively capture of APOC-III in order to reduce the activation of lipoprotein lipase inhibition during hypertriglyceridemia treatment. The zeolite nanoparticles can be adapted to hemophilic patients (hemophilia A (F-VIII deficient) and hemophilia B (F-IX deficient)) with a risk of bleeding, and thus might be potentially used in combination with the existing therapy.

Zeolites are low-density crystalline aluminosilicates possessing regular micropores (one-, two- and three-dimensional) with well-defined pore sizes and shapes. The well-defined structures of zeolites combine with hydrophilic/hydrophobic and porous nature render them as useful shape-selective molecular sieves and hosts for various guest molecules (organic and inorganic). A significant effort has been devoted to the preparation of zeolites with nanometer dimensions with enhanced accessibility of reactant molecules in order to achieve higher product yield/selectivity in catalytic reactions or fast diffusion in adsorption and ion exchanged processes[1,2]. In addition to the regular micropores, the zeolites nanoparticles contain meso- and macro-pores due to the close packing of homogeneous in size and morphology crystals. Additionally, the zeolite nanoparticles with a size smaller than 200 nm can be stabilized in suspensions with different concentrations that are colloidal stable and do not agglomerate with time[2].

[1]Faculty of Science, University of Groningen, University Medical Center Groningen, Groningen, the Netherlands. [2]School of Chemical Sciences, University Sains Malaysia, 11800 USM, Malaysia. [3]Department of Plasma Proteins, Sanquin Research, Amsterdam, The Netherlands. [4]Department of Experimental Vascular Medicine, Academic Medical Center, Amsterdam, the Netherlands. [5]Institute for Liver and Digestive Health, Division of Medicine, University College London (UCL), London, United Kingdom. [6]Laboratory of Catalysis and Spectroscopy, ENSICAEN, University of Caen, CNRS, 6 Boulevard du Maréchal Juin, 14050 Caen, France. [7]University of Groningen, University Medical Center Groningen, Department Bioengineering, Groningen, the Netherlands. [8]Department of Chemistry, Institute for Advanced Studies in Basic Sciences (IASBS), Iran. [9]University of Groningen, University Medical Center Groningen, Department Cell Biology, Department medical proteomics, Groningen, the Netherlands. [10]Department of Clinical Genetics, Academic Medical Center, Amsterdam, the Netherlands. [11]Department of Gastroenterology and Hepatology, Erasmus Medical Center, Rotterdam, the Netherlands. [12]Division of Cardiovascular Medicine, School of Medicine, Stanford University, Stanford, California, USA. [13]Cardiovascular Institute, School of Medicine, Stanford University, Stanford, California, USA. *These authors contributed equally to this work. Correspondence and requests for materials should be addressed to F.R. (email: f.rezaee@erasmusmc.nl or f.rezaee@med.umcg.nl)

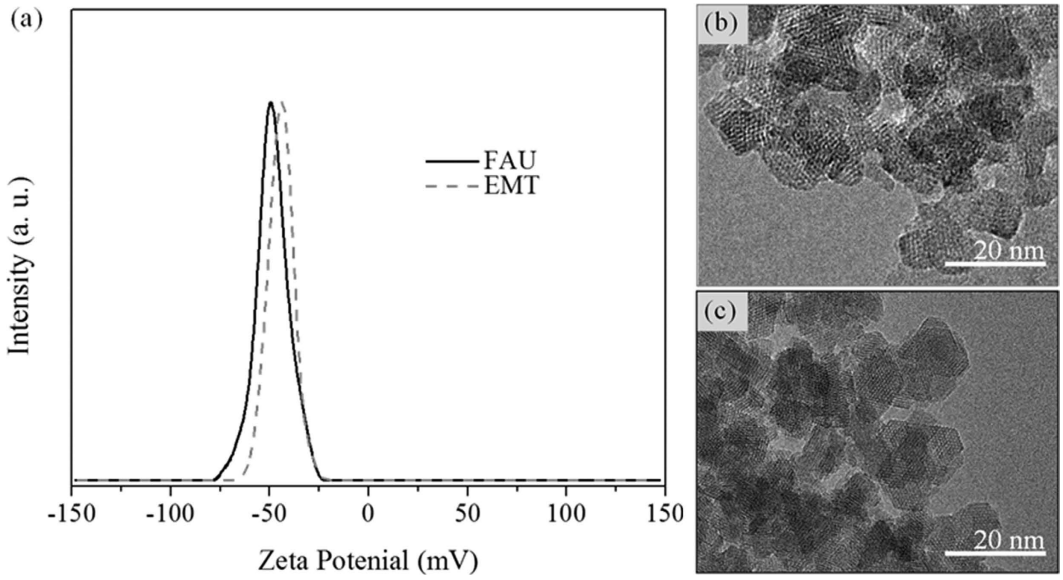

Figure 1. (**a**) Zeta potential curves of EMT- and FAU-zeolite suspensions, and transmission electron micrographs of (**b**) EMT- and (**c**) FAU-zeolite nanoparticles.

Therefore, aluminosilicate and pure silicate zeolite nanoparticles are safely applied in protein adsorption for organ transplantation[3], hemostatic material for wound healing[4], MRI contrasting agent[5], antibacterial agents[6] and drug delivery[7]. Moreover, the immobilization of biomolecules on the well-developed external surface of zeolite nanoparticles is the focus of intense activity in biotechnology and biomedicine[8–10].

EMT- and FAU-type zeolites have very low framework density (FD = 12.7–12.9 T/1000 Å), high porosity, diverse morphology and crystal sizes[11]. Unlike its cubic FAU polymorph that has only supercages (1.15 nm^3), the EMT-zeolite has two cages: hypocage (0.61 nm^3) and hypercage (1.24 nm^3) due to different stacking of faujasite sheets. As a result, it creates different catalytic and sorption properties for both materials[11].

Recently, it was reported that the large pore EMT-type nanosized zeolite can adsorb fibrinogen and apolipoproteins while keeping the same amount of albumin in human plasma[12]. Fibrinogen is a very complex, hydrophilic and bipolar molecule[13–18]. In opposite to fibrinogen, apolipoprotein C-III (APOC-III) is a simple, highly hydrophobic and non-polar molecule with a molecular weight of approximately 11 kDa. APOC-III inhibits very low-density lipoproteins (VLDL)-triglycerides, hepatic lipase (HL), and lipoprotein lipase (LPL) functions; the major function of LPL is to hydrolyze chylomicrons (CMs). As a result, the inhibition of LPL leads in the delay of degradation of triglyceride-rich particles (i.e. CM and VLDL), which is implicated in pathophysiological events such as cardiovascular diseases[19–24].

The adsorption specificity of proteins has been studied for several nanoparticles including gold, super paramagnetic iron oxide, silica, and polystyrene[25–30]. However, to our best knowledge, the adsorption specificity of proteins on zeolite nanoparticles has not been investigated so far. As a result, it hampers the development of rational targets for biomedical applications of zeolite nanoparticles.

The aim of this paper is to study the selective sorption behavior of nanosized EMT- and FAU-zeolites for human plasma proteins with different concentrations of either the zeolites or the human plasma proteins.

Results

Characterization of EMT- and FAU-zeolite nanoparticles. High-resolution transmission electron microscopy (HR-TEM) and dynamic light scattering (DLS) were used to study the size and morphology of the zeolite nanocrystals. Discrete octahedral FAU- and hexagonal EMT- zeolite nanocrystals with an average diameter in the range of 8–12 nm are shown in Figure 1. Both the EMT- and FAU- zeolite nanocrystals have well developed crystalline faces. Moreover they appear as single crystals, and no crystals intergrowth was observed, which is in a good accordance with the zeta potential measurements and scanning electron microscopy study (Figure S1). The zeta potential values measured for the EMT- and FAU- zeolite nanoparticles of −44 and −50 mV, respectively, correspond to colloidal samples containing highly stable non-agglomerated crystals (Figure 1). On the other side the negative zeta potential value represent particles with negative surface charge. The surface charges of the zeolite nanoparticles are expected to play an important role in the interactions with human plasma proteins. Therefore the surface charge and charge density of both zeolite nanoparticles were determined. Both samples have almost identical surface charge density, i.e., −0.50 mC/m^2 and −0.58 mC/m^2 for EMT- and FAU- zeolite crystals respectively (Table 1a), while the surface charge of FAU- zeolite nanoparticles is higher (−299 mC/g)

Zeolites	Si/Al ratio	Chemical composition	SBET (m^2/g)[a]	$S_{External}$ (m^2/g)[b]	V_{Total} (cm^3/g)[c]	Surface charge (mC/g)	Surface charge density (mC/m^2)	Zeta potential (mV)
(a) Physicochemical properties of EMT- and FAU- type zeolites. [a]Specific BET surface area; [b]External surface area; [c]Total pore volume								
EMT	1.18	$Na_{88}(AlO_2)_{88}(SiO_2)_{104}$	570	220	0.89	−235	−0.50	−44
FAU	1.63	$Na_{73}(AlO_2)_{73}(SiO_2)_{119}$	845	235	1.27	−229	−0.58	−50

Accession	Description	Mw	−10lgP		Spectra		NpSpCk		Average NpSpCk
			S 1	S 2	S 1	S 2	S 1	S 2	
(b) (12% EMT + 100% human plasma)									
P02656|APOC3_HUMAN	Apolipoprotein C-III OS = Homo sapiens GN = APOC3 PE = 1 SV = 1	10852	189.29	177.2	5	6	27.59	25.75	26.67
P02671|FIBA_HUMAN	Fibrinogen alpha chain OS = Homo sapiens GN = FGA PE = 1 SV = 2	94973	414.34	334.15	29	29	18.28	14.22	16.25
P02679|FIBG_HUMAN	Fibrinogen gamma chain OS = Homo sapiens GN = FGG PE = 1 SV = 3	51512	314.11	283.84	13	14	15.11	12.66	13.88
P02675|FIBB_HUMAN	Fibrinogen beta chain OS = Homo sapiens GN = FGB PE = 1 SV = 2	55928	284.67	200.7	9	13	9.64	10.83	10.23
P02768|ALBU_HUMAN	Serum albumin OS = Homo sapiens GN = ALB PE = 1 SV = 2	69367	326.93	334.97	11	16	9.50	10.74	10.12
P02647|APOA1_HUMAN	Apolipoprotein A-I OS = Homo sapiens GN = APOA1 PE = 1 SV = 1	30778	160.72	166.71	2	5	3.89	7.57	5.73
P19823|ITIH2_HUMAN	Inter-alpha-trypsin inhibitor heavy chain H2 OS = Homo sapiens GN = ITIH2 PE = 1 SV = 2	106463	130.81	229.14	7	8	3.94	3.50	3.72
P04004|VTNC_HUMAN	Vitronectin OS = Homo sapiens GN = VTN PE = 1 SV = 1	54306	198.44	111.32	3	3	3.31	2.57	2.94
P01024|CO3_HUMAN	Complement C3 OS = Homo sapiens GN = C3 PE = 1 SV = 2	187147	373.99	365.84	9	11	2.88	2.74	2.81
P04003|C4BPA_HUMAN	C4b-binding protein alpha chain OS = Homo sapiens GN = C4BPA PE = 1 SV = 2	67033	92.93	53.7	2	2	1.79	1.39	1.59
P01857|IGHG1_HUMAN	Ig gamma-1 chain C region OS = Homo sapiens GN = IGHG1 PE = 1 SV = 1	36106	ND	96.97	0	2	0.00	2.58	1.29
P04114|APOB_HUMAN	Apolipoprotein B-100 OS = Homo sapiens GN = APOB PE = 1 SV = 2	515611	238.42	208.01	10	9	1.16	0.81	0.99
P02748|CO9_HUMAN	Complement component C9 OS = Homo sapiens GN = C9 PE = 1 SV = 2	63173	ND	62.79	0	2	0.00	1.47	0.74
P00751|CFAB_HUMAN	Complement factor B OS = Homo sapiens GN = CFB PE = 1 SV = 2	85533	45.2	ND	2	0	1.40	0.00	0.70
P02787|TRFE_HUMAN	Serotransferrin OS = Homo sapiens GN = TF PE = 1 SV = 3	77064	36.21	95.17	1	1	0.78	0.60	0.69
P02749|APOH_HUMAN	Beta-2-glycoprotein 1 OS = Homo sapiens GN = APOH PE = 1 SV = 3	38298	ND	55.03	0	1	0.00	1.22	0.61
P00736|C1R_HUMAN	Complement C1r subcomponent OS = Homo sapiens GN = C1R PE = 1 SV = 2	80119	74.95	ND	1	0	0.75	0.00	0.37
P07358|CO8B_HUMAN	Complement component C8 beta chain OS = Homo sapiens GN = C8B PE = 1 SV = 3	67047	ND	76.88	0	1	0.00	0.69	0.35
P01042|KNG1_HUMAN	Kininogen-1 OS = Homo sapiens GN = KNG1 PE = 1 SV = 2	71957	ND	44.95	0	1	0.00	0.65	0.32
(c) (12% FAU + 100% human plasma)									
P02656|APOC3_HUMAN	Apolipoprotein C-III OS = Homo sapiens GN = APOC3 PE = 1 SV = 1	10852	259.65	263.71	12	6	22.68	23.56	23.12
P02679|FIBG_HUMAN	Fibrinogen gamma chain OS = Homo sapiens GN = FGG PE = 1 SV = 3	51512	384.9	282.85	27	11	10.75	9.10	9.92
P02671|FIBA_HUMAN	Fibrinogen alpha chain OS = Homo sapiens GN = FGA PE = 1 SV = 2	94973	367.67	281.85	43	23	9.29	10.32	9.80
P02768|ALBU_HUMAN	Serum albumin OS = Homo sapiens GN = ALB PE = 1 SV = 2	69367	372.84	333.91	34	15	10.05	9.21	9.63
P02675|FIBB_HUMAN	Fibrinogen beta chain OS = Homo sapiens GN = FGB PE = 1 SV = 2	55928	340.52	209.02	22	11	8.07	8.38	8.22
P19827|ITIH1_HUMAN	Inter-alpha-trypsin inhibitor heavy chain H1 OS = Homo sapiens GN = ITIH1 PE = 1 SV = 3	101389	378.57	407.28	28	21	5.66	8.82	7.24
P19823|ITIH2_HUMAN	Inter-alpha-trypsin inhibitor heavy chain H2 OS = Homo sapiens GN = ITIH2 PE = 1 SV = 2	106463	365.4	346.93	21	22	4.05	8.80	6.42
P04004|VTNC_HUMAN	Vitronectin OS = Homo sapiens GN = VTN PE = 1 SV = 1	54306	251.16	262.66	10	5	3.78	3.92	3.85

Continued

P02647|APOA1_HUMAN	Apolipoprotein A-I OS = Homo sapiens GN = APOA1 PE = 1 SV = 1	30778	166.81	161.68	5	2	3.33	2.77	3.05
P00747|PLMN_HUMAN	Plasminogen OS = Homo sapiens GN = PLG PE = 1 SV = 2	90569	233.27	171.78	8	8	1.81	3.76	2.79
P01024|CO3_HUMAN	Complement C3 OS = Homo sapiens GN = C3 PE = 1 SV = 2	187147	426.87	386.41	20	12	2.19	2.73	2.46
P02649|APOE_HUMAN	Apolipoprotein E OS = Homo sapiens GN = APOE PE = 1 SV = 1	36154	170.95	ND	4	0	2.27	0.00	1.13
P02760|AMBP_HUMAN	Protein AMBP OS = Homo sapiens GN = AMBP PE = 1 SV = 1	39000	ND	58.57	0	2	0.00	2.18	1.09
P0C0L4|CO4A_HUMAN	Complement C4-A OS = Homo sapiens GN = C4A PE = 1 SV = 1	192770	203.76	143.77	8	5	0.85	1.11	0.98
P0C0L5|CO4B_HUMAN	Complement C4-B OS = Homo sapiens GN = C4B PE = 1 SV = 1	192792	203.76	143.77	8	5	0.85	1.10	0.98
P01042|KNG1_HUMAN	Kininogen-1 OS = Homo sapiens GN = KNG1 PE = 1 SV = 2	71957	135.73	78.39	4	1	1.14	0.59	0.87
P02765|FETUA_HUMAN	Alpha-2-HS-glycoprotein OS = Homo sapiens GN = AHSG PE = 1 SV = 1	39325	183.38	ND	3	0	1.56	0.00	0.78
P00450|CERU_HUMAN	Ceruloplasmin OS = Homo sapiens GN = CP PE = 1 SV = 1	122205	134.61	71.87	5	2	0.84	0.70	0.77
P04114|APOB_HUMAN	Apolipoprotein B-100 OS = Homo sapiens GN = APOB PE = 1 SV = 2	515611	232.58	238.32	12	12	0.48	0.99	0.73
P35542|SAA4_HUMAN	Serum amyloid A-4 protein OS = Homo sapiens GN = SAA4 PE = 1 SV = 2	14747	124.34	ND	1	0	1.39	0.00	0.70
P07358|CO8B_HUMAN	Complement component C8 beta chain OS = Homo sapiens GN = C8B PE = 1 SV = 3	67047	160.9	ND	4	0	1.22	0.00	0.61
P00751|CFAB_HUMAN	Complement factor B OS = Homo sapiens GN = CFB PE = 1 SV = 2	85533	98.7	ND	5	0	1.20	0.00	0.60
P04196|HRG_HUMAN	Histidine-rich glycoprotein OS = Homo sapiens GN = HRG PE = 1 SV = 1	59578	45.77	ND	3	0	1.03	0.00	0.52
P07360|CO8G_HUMAN	Complement component C8 gamma chain OS = Homo sapiens GN = C8G PE = 1 SV = 3	22277	94.8	ND	1	0	0.92	0.00	0.46
P00738|HPT_HUMAN	Haptoglobin OS = Homo sapiens GN = HP PE = 1 SV = 1	45205	36.07	ND	2	0	0.91	0.00	0.45
P13671|CO6_HUMAN	Complement component C6 OS = Homo sapiens GN = C6 PE = 1 SV = 3	104786	ND	56.49	0	2	0.00	0.81	0.41
Q9H6K5|YS027_HUMAN	Putative uncharacterized protein FLJ22184 OS = Homo sapiens PE = 1 SV = 1	60039	35.56	ND	2	0	0.68	0.00	0.34
P04003|C4BPA_HUMAN	C4b-binding protein alpha chain OS = Homo sapiens GN = C4BPA PE = 1 SV = 2	67033	ND	31.62	0	1	0.00	0.64	0.32
P00748|FA12_HUMAN	Coagulation factor XII OS = Homo sapiens GN = F12 PE = 1 SV = 3	67792	90.73	ND	2	0	0.61	0.00	0.30
P08603|CFAH_HUMAN	Complement factor H OS = Homo sapiens GN = CFH PE = 1 SV = 4	139096	111.35	ND	4	0	0.59	0.00	0.29
P02749|APOH_HUMAN	Beta-2-glycoprotein 1 OS = Homo sapiens GN = APOH PE = 1 SV = 3	38298	72.34	ND	1	0	0.54	0.00	0.27
P06396|GELS_HUMAN	Gelsolin OS = Homo sapiens GN = GSN PE = 1 SV = 1	85697	ND	36.85	0	1	0.00	0.50	0.25
Q14410|GLPK2_HUMAN	Glycerol kinase 2 OS = Homo sapiens GN = GK2 PE = 2 SV = 2	60594	34.37	ND	1	0	0.34	0.00	0.17
P00734|THRB_HUMAN	Prothrombin OS = Homo sapiens GN = F2 PE = 1 SV = 2	70037	64.19	ND	1	0	0.29	0.00	0.15
P00736|C1R_HUMAN	Complement C1r subcomponent OS = Homo sapiens GN = C1R PE = 1 SV = 2	80119	79.24	ND	1	0	0.26	0.00	0.13
P49815|TSC2_HUMAN	Tuberin OS = Homo sapiens GN = TSC2 PE = 1 SV = 2	200607	27.34	ND	2	0	0.20	0.00	0.10
Q96L96|ALPK3_HUMAN	Alpha-protein kinase 3 OS = Homo sapiens GN = ALPK3 PE = 2 SV = 2	201270	37.91	ND	1	0	0.10	0.00	0.05
P02751|FINC_HUMAN	Fibronectin OS = Homo sapiens GN = FN1 PE = 1 SV = 4	262622	42.55	ND	1	0	0.08	0.00	0.04

Table 1. NLC-MS/MS combined with PEAKS DB analysis of the corona (protein content) and physicochemical properties of zeolite nanoparticles (NPs). Table 1a shows physicochemical surface properties of EMT and FAU zeolite NPs. Table 1b represents EMT zeolite NPs (12% EMT + 100% human plasma) and Table 1c is FAU zeolite NPs (12% FAU + 100% human plasma). The accession number, gene name, species (Human), protein description, identification score (-10lgP), molecular weight (Mw) in kDa, total spectra per protein of EMT (12%) and FAU (12%) zeolite NPs incubated with human plasma (100%), together with their relative amount (NpSpCk value). Sample (S). All protein coverage of different combination (EMT (%) and plasma (%), and (FAU (%) and plasma (%)) were reported in Supplementary Information.

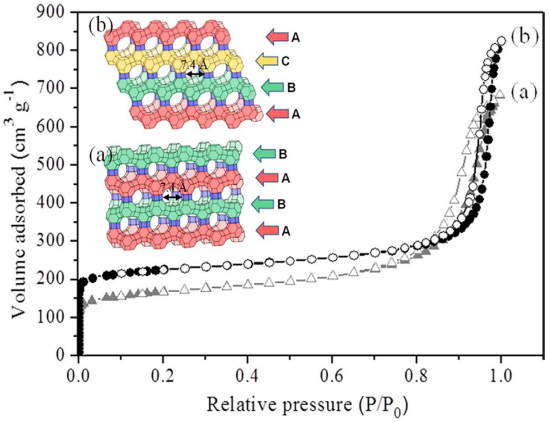

Figure 2. Nitrogen adsorption (closed symbol) and desorption (open symbol) isotherms of (**a**) EMT- and (**b**) FAU-zeolite nanoparticles. *Inset:* schematic presentation of the framework type of (a) EMT- and (b) FAU-zeolites, which can be described by the stacking of sodalite layers, resulting in ABABAB and ABCABC sequences, respectively.

than the EMT- zeolite (−235 mC/g) (Table 1a). This can be explained with the different specific surface area of the EMT- and FAU- zeolite nanocrystals (Table 1a). The surface charge of the zeolite nanoparticles is negative, which is consistent with their high hydrophilicity. Additionally, the porosity of the zeolite nanocrystals was evaluated by nitrogen sorption measurements carried out at −196 °C (Figure 2). The N_2 sorption isotherms of both samples resembled Type I and Type IV isotherms, indicating the presence of micropores and mesopores (textural porosity); the mesopores with an average diameter of 25 nm are originated from the close packing of the zeolite nanocrystals. The results extracted from the N_2 sorption isotherms for EMT- and FAU- zeolite nanoparticles are summarized in Table 1. The BET specific surface area of FAU- zeolite nanoparticles is 845 m^2/g, which is higher than for the EMT- zeolite nanoparticles (570 m^2/g). The external surface area of EMT- and FAU-zeolite nanoparticles is 220 m^2/g and 235 m^2/g, respectively, which contributed of approximately 30 - 40% of their specific surface area. In addition, both samples have high total pore volume, i.e., for the EMT zeolite is 0.89 cm^3/g and for the FAU zeolite is 1.27 cm^3/g, which will be further beneficial for the selective sorption toward human plasma proteins.

Semi-quantitative assessment of corona protein composition of EMT- and FAU- zeolite nanoparticles. Semi-quantitative equation is used to obtain information about the amount of each protein bound onto the surface of the EMT- and FAU- zeolite nanoparticles. All proteins identified in the experiments are described in Supporting Information (SI). The semi-quantitative assessment of each protein, namely, the normalized percentage of the spectral count for protein k ($NpSpC_k$), is determined based on the total number of all peptides that were attributed to a matched protein in the nLC-MS/MS spectra (Tables 1b,c; and SI: Tables S1 and S2).

The affinity of the EMT- and FAU- zeolite nanoparticles towards human plasma proteins was investigated by incubating zeolite nanoparticles with plasma proteins using one of the following strategies: (1) the concentration of nanoparticles was kept constant but the plasma concentration was varied, and (2) the plasma concentration was kept constant but the concentration of zeolite nanoparticles was varied. The identification of proteins present on the surface of EMT- and FAU-zeolite nanoparticles (SI: Tables S1 and S2) was carried out using nLC-MS/MS (LTQ-ORBITRAP-XL; tandem mass spectrometry) combined with PEAKS DB (software) analysis. The nLC-MS/MS results show that with increasing the plasma concentrations from 10% to 100%, the APOC-III and the three chains of fibrinogen (FIBA, FIBB and FIBG) are bound on the surface of the zeolite nanoparticles. The amount of adsorption was less dependent on the concentration of zeolite nanoparticles than plasma concentrations used (Figures 3 and 4; and SI: Tables S1 and S2). After exposure of zeolite nanoparticles to very low plasma concentrations (10%), the zeolites exhibit a high affinity for immunoglobulin gamma (i.e. IGHG1, IGHG2 and IGHG4) as compared to the high plasma concentrations (Figures 3 and 4). Notably, upon using EMT-zeolite nanoparticles with 100% plasma, the APOC-III showed an adsorption of 30%. Furthermore, all three chains of fibrinogen (FIBA, FIBB, and FIBG) demonstrated a high affinity toward EMT-zeolite nanoparticles even at low concentrations (4–12%) incubated with 10% plasma. As a representative example, the spectra of Fibrinogen α-chain and APOC-III after injection of the extracted peptides from EMT and FAU zeolite nanoparticles are depicted in Figure 5 (a,b).

Interaction of APOC-III and fibrinogen with EMT- and FAU-zeolite nanoparticles. The APOC-III is adsorbed on the surface of both EMT- and FAU-zeolite nanoparticles (Figure S2). The positively charged amino acid residues of APOC-III and the negatively charged EMT- and FAU-zeolite

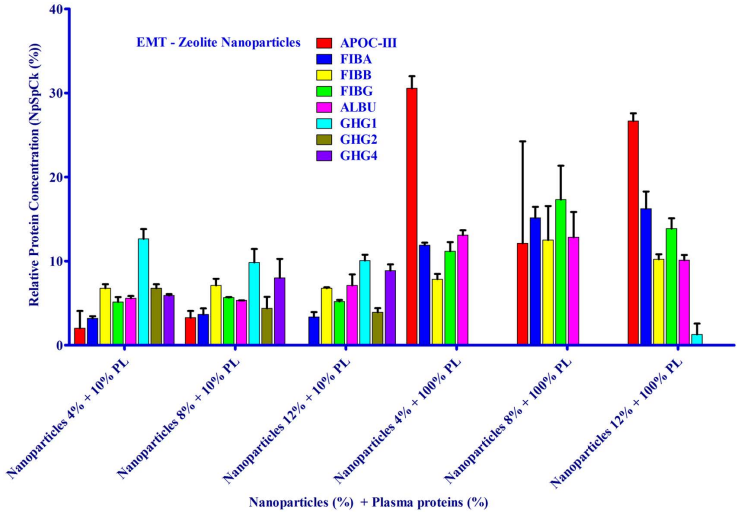

Figure 3. nLC-MS/MS analysis of corona-associated proteins on EMT-zeolite nanoparticles. Apolipoprotein C-III (APOC-III), fibrinogen alpha chain (FIBA), fibrinogen beta chain (FIBB), fibrinogen gamma chain (FIBG), albumin (ALBU), IGHG1, IGHG2 and IGHG4.

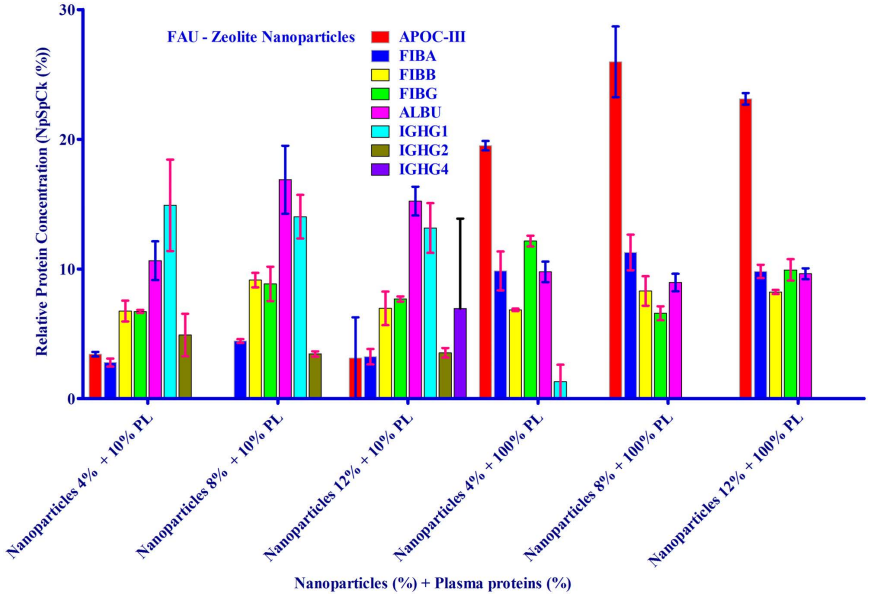

Figure 4. nLC-MS/MS analysis of corona-associated proteins on FAU-zeolite nanoparticles. Apolipoprotein C-III (APOC-III), fibrinogen alpha chain (FIBA), fibrinogen beta chain (FIBB), fibrinogen gamma chain (FIBG), albumin (ALBU), IGHG1, IGHG2 and IGHG4.

nanoparticles facilitate the electrostatic interactions and thus the adsorption of APOC-III on the zeolite surfaces. Fibrinogen is a bipolar molecule with negatively charged E and D domains, and positively charged αC-domain (PDB entry: 3GHG; Figure 6a). The αC-domain of fibrinogen Aα-chain (starts from amino acid 392 to 610) is highly flexible, mobile and positively charged[31–34]. This region shows positive electrostatic character, which is potentially responsible for the interaction between the fibrinogen and the negatively charged EMT- and FAU-zeolite nanoparticles. A schematic diagram of human fibrinogen structure and a flexible αC-domain of the fibrinogen are depicted in Figure 6b.

Effect of EMT- and FAU-zeolite nanoparticles on blood coagulation. Fibrinogen is a glycoprotein that helps in the formation in blood clots. Since the fibrinogen has strong tendency to bind to both zeolite nanoparticles, thus it is very important to investigate their effect on clotting time. In respect to this, coagulometer was applied to determine prothrombin time (PT), i.e., a test that measures how long it takes the blood to clot. Without adding zeolite nanoparticles, the thrombin time is 23 sec (Figure 7).

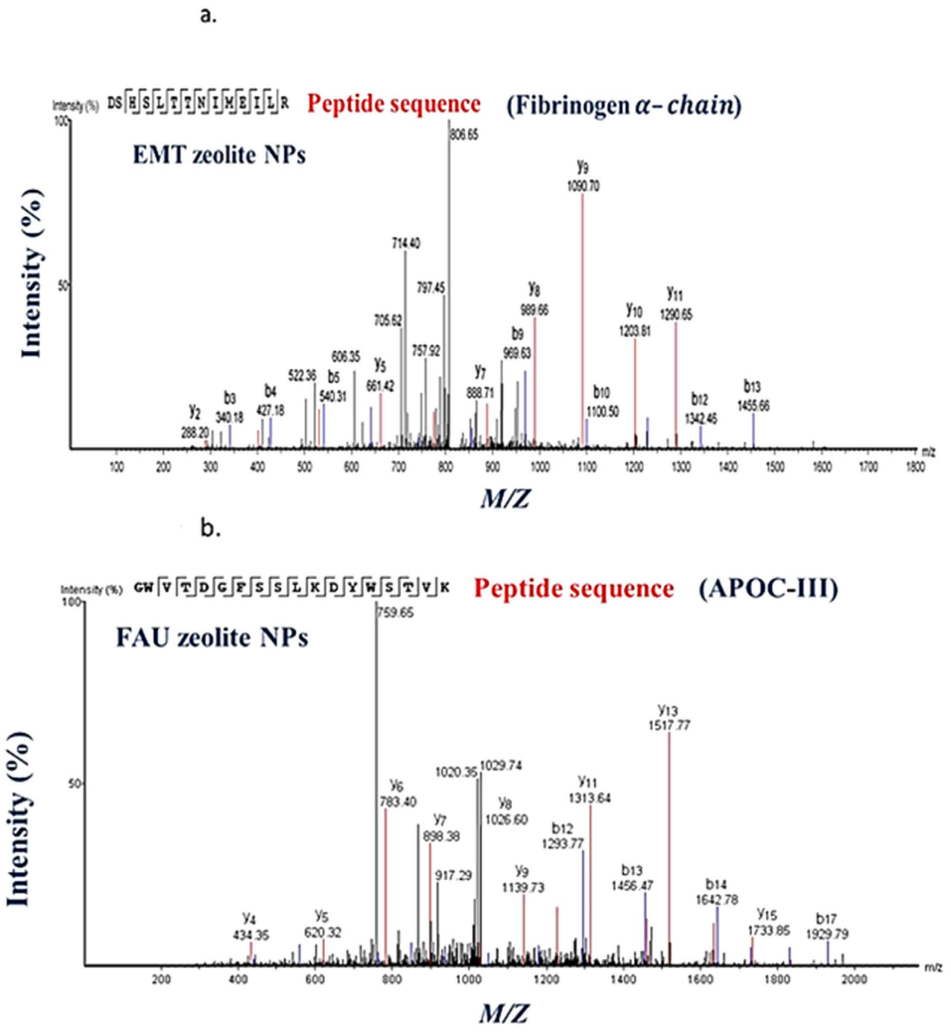

Figure 5. Representative nLC-MS/MS spectra of (**a**) fibrinogen α-chain after injection of extracted peptides from EMT- zeolite nanoparticles, and (**b**) APOC-III after injection of extracted peptides from FAU- zeolite nanoparticles. The peptide sequence derived from the two spectra are **GWVTDGFSSLKDYWSTVK** (APOC-III) and **DSHSLTTNIMEILR** (fibrinogen α-chain), respectively.

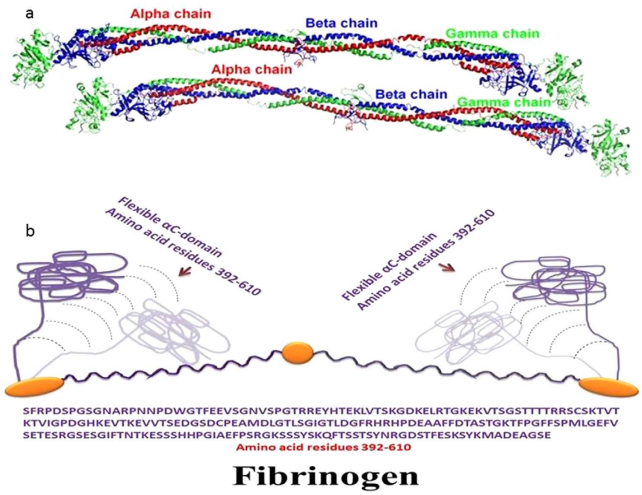

Figure 6. (**a**) Crystal structure of fibrinogen (crystal structure was used from PDB entry 3GHG), (**b**) schematic diagram of fibrinogen structure showing the flexibility of positively charged αC-domain. The amino acid sequence of αC-domain, amino acid residues 392–610, is shown below the diagram.

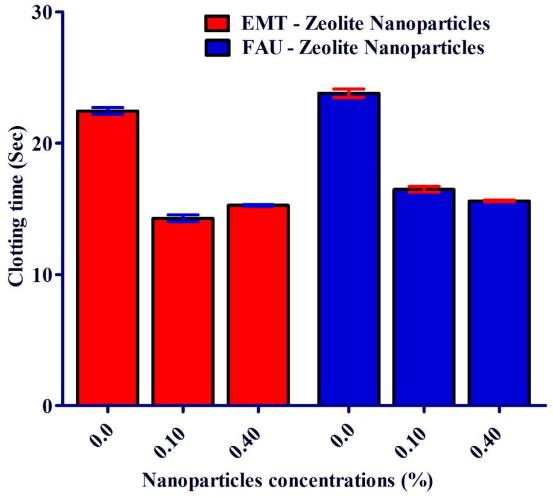

Figure 7. The effect of EMT- and FAU-zeolite nanoparticles on clotting time: prothrombin test (PT) is performed in pooled plasma with and without EMT- and FAU-zeolite nanoparticles (incubation for 30 min) in KC-10 coagulometer. Clotting time is expressed in seconds (Sec). Zeolite nanoparticles (0.1% and 0.4%) are incubated in 100 μl of 100% pooled plasma.

Upon treatment of 50% plasma for 30 min with 0.1% EMT- and FAU-zeolite nanoparticles, the clotting time is shortened with 5–7 seconds. One of the possibilities could be potentially due to the adsorption of fibrinogen to zeolite nanoparticles in the pooled plasma and hence, enhancing the rate of clot formation. The FAU-zeolite nanoparticles with higher surface area, higher total pore volume and higher surface charge density show clotting time of 18 sec, while for the EMT- zeolite nanoparticles is 16 sec. This indicates that EMT-zeolite nanoparticles with higher hydrophilicity (Si/Al ratio of 1.14) are more selectively in interacting with the fibrinogens and leads to enrichment of fibrinogens in blood, which is essential in blood clotting. Thus, these NPs accelerate the time of blood clot formation and the mechanism whereby these NPs accelerate coagulation remains to be elucidated.

Discussion

Nanosized EMT- and FAU-zeolites open the possibility to use them in new biological and clinical applications (biological fluid)[35–37]. Of note, proteins are one of the most important components of biological fluid such as plasma system (sub-fraction of blood) and the interactions with zeolite nanoparticles is important to be studied prior further use.

There are ignorable differences in the number of identified proteins bound on the surface of the EMT- and FAU-zeolite nanoparticles (at 4% NPs) when they were exposed to 10% plasma proteins, and this could be due to (1) the low abundant proteins present in diluted plasma, and (2) no real competition between proteins during the adsorption on zeolite nanoparticles with large external surface. The latter phenomenon could be mediated by the presence of a few very high-abundance proteins albumin and immunoglobulin G (IgG)[38–40], which are responsible for the constitution of 70% and 20% of plasma proteins, respectively. This is the reason why the two major proteins in the EMT- and FAU-corona (protein layer of nanoparticles) exposed to 10% plasma only are albumin and IgG. It should be noted that the two major functions of albumin are binding and transporting the materials[41]. Importantly, the number of proteins present in the corona of zeolite nanoparticles is much less at 100% plasma exposure (*in vivo* state) than with 10% plasma. Therefore the assumption that there is a competition between proteins to occupy the corona of the zeolite nanoparticles is reasonable. Thus, the protein composition of corona in EMT- and FAU-zeolite nanoparticles appeared to be more dependent on plasma concentration and the type of zeolite (e.g. may be the external surface area of zeolite crystals) than NPs concentrations with respect to APOC-III, IGHG1, IGHG2 and IGHG3. Since EMT-zeolite nanoparticles are more hydrophilic than FAU-zeolite nanoparticles, it is possible to assume that the high adsorption on EMT- zeolite may be due to the hydrophilicity.

Selective adsorption of APOC-III and fibrinogen on the surface of EMT- and FAU-zeolite nanoparticles. The selective adsorption of APOC-III on the surface of EMT- and FAU-zeolite nanoparticles is most likely *via* electrostatic interactions between the solvent exposed positively charged amino acid residues of APOC-III and the negatively charged EMT- and FAU-zeolites. Specifically, there are two regions in the structures of APOC-III, that the side chains of amino acid residues are solvent exposed, and thus they can electrostatically interact with the negatively charged zeolite nanocrystals (Figure S2). The region including amino acid residues *Lys17*, *His18*, *Lys21* and *Lys24*, and the area containing the

solvent exposed amino acid residues *Lys51, Lys58* and *Lys60* are highly effective in binding to the negatively charged EMT- and FAU-zeolite nanoparticles[42]. Furthermore, APOC-III is an inhibitor of LPL activation and it is considered as a risk factor for cardiovascular diseases. The two types zeolites can potentially be used for selectively capture of APOC-III, and to reduce the activation of lipoprotein lipase inhibition in hypertriglyceridemia treatment.

The application of *in vivo* plasma proteins (i.e. 100%) appeared to be essential for a strong binding of fibrinogen (all three chains) to the EMT- and FAU-zeolite nanoparticles. Fibrinogen D and E domains are rich in aspartic acid (*Asp*) and glutamic acid (*Glu*) residues, and these sections are negatively charged. In contrast, the αC-domain (remaining part of carboxyl terminal of both alpha chains, which are not present in D domain) is positively charged because this region is rich in arginine (*Arg*) and lysine (*Lys*). The fibrinogen is a dipolar molecule and it can be one of the potential reasons that facilitate the adsorption of fibrinogen on the surface of negatively charged EMT- and FAU-zeolite nanoparticles. Importantly, a maximum concentration of fibrinogen is a guarantee for its strong adsorption to both zeolite nanoparticles. Since these two nanoparticles are negatively charged, it is possible that fibrinogen is linked to the surface of the zeolite nanoparticles *via* αC-domains, which are positively charged. Other possibility is that the fibrinogen molecules, which are dipolar (D and E domains are negatively charged and αC-domain positively charged) and very stable, and hold tightly together. Most likely, the positive charged fibrinogen domain binds to the zeolite nanoparticles.

Effect of EMT- and FAU-zeolite nanoparticles on coagulation. It is very important to shed light on the role of the zeolite nanoparticles in biological functions such as coagulation system, which play an important role in wound healing process. Since the EMT- and FAU-zeolite nanoparticles show a very high selectivity for fibrinogen, it is necessary to measure the effect of these zeolite nanoparticles on fibrin formation. Notably, both zeolite nanoparticles accelerate the fibrin forming process. This property of the EMT- and FAU-zeolite nanoparticles can be adapted to hemophilic patients (hemophilia A (F-VIII deficient) and hemophilia B (F-IX deficient)) with a risk of bleeding. The present therapy of such patients is based on treatment with F-VIII extracts. Thus, the EMT- and FAU-zeolite nanoparticles might be potentially used as a complementary therapy in combination with the existing one.

Conclusions

This study provides an evidence for high specific adsorption of APOC-III and fibrinogen on EMT- and FAU-zeolite nanoparticles. There are three factors, that determine the protein content of corona; 1- plasma concentrations, 2- the type of zeolite NPs (external surface area and hydrophilicity of zeolite nanocrystals), and 3- NPs concentrations (but less effect). Moreover, it was found that these NPs accelerate the time of blood clot formation, which can be adapted to hemophilic patients (hemophilia A (F-VIII deficient) and hemophilia B (F-IX deficient)) with a risk of bleeding, and thus might be potentially used in combination with the existing therapy. Also, the zeolite nanoparticles can potentially be used for selectively capture of APOC-III in order to reduce the activation of lipoprotein lipase inhibition during hypertriglyceridemia treatment.

Experimental section

Synthesis and characterization of EMT- and FAU-zeolite nanoparticles. The EMT-zeolite nanoparticles with a diameter of 8–12 nm were synthesized from a clear precursor suspension with a molar composition of $18.45Na_2O$: $5.15SiO_2$: $1Al_2O_3$: $240.3H_2O$[35]. This suspension was subjected to hydrothermal synthesis at 30 °C for 36 h. The crystalline EMT-zeolite nanoparticles were then purified by a high-speed centrifugation (75465 × g for 2 h) and re-dispersed in double distilled water; this procedure was repeated six times until the final colloidal suspension has a pH of 7.0; the solid concentration of EMT-zeolite nanoparticles was adjusted to 5 wt%.

The FAU-zeolite nanoparticles with a diameter of 8–12 nm were synthesized from a clear precursor suspension with a molar composition: $9Na_2O$: $10SiO_2$: $0.7Al_2O_3$: $160H_2O$[43]. The suspension was subjected to hydrothermal synthesis at 50 °C for 45 h. The FAU-zeolite nanoparticles were then purified by a high-speed centrifugation (75465 × g for 2 h) and re-dispersed in double distilled water; this procedure was repeated three times until the final colloidal suspensions have a pH of 7.0; the solid concentration of FAU-nanoparticles was then adjusted to 5 wt%.

The chemical compositions of zeolite nanocrystals were determined by X-ray fluorescence (XRF) spectroscopy using a MagiX PHILIPS PW2540FEI. Transmission electron microscope (TEM) and scanning electron microscope (SEM) operating at 300 kV and 30 kV using a JEOL and a Philips XL-30, respectively were applied to study the crystalline EMT- and FAU-zeolite nanoparticles. The hydrodynamic diameters and zeta potential of the zeolite nanoparticles in the suspensions were determined with a Malvern Zetasizer Nano. The samples were first re-suspended in 10 mL of 1.0 mM KCl and the zeta potential of the particles was recorded. The surface charge density, σ, is calculated from the Grahame equation[44]:

$$\sigma = \sqrt{8\varepsilon\varepsilon_0 T}\ \sinh\left(\frac{e\Psi_0}{2k_B T}\right) \times \sqrt{M_{1:1} N_A} \quad (1)$$

where, $\varepsilon\varepsilon_0$ is the dielectric permittivity of zeolite (FAU = 1.3458×10^{-11} AsV^{-1} m^{-1}, EMT = 1.3547×10^{-11} AsV^{-1} m^{-1}), k_B is the Boltzmann constant (1.381×10^{-23} JK^{-1}), ψ_0 is the surface potential or zeta potential of the zeolite suspensions in 1.0 mM KCl, e is the electronic charge (1.602×10^{-19} C), T is the absolute temperature (298 K), N_A is the Avogadro's number (6.022×10^{23} mol^{-1}) and $M_{1:1}$ is the concentration of KCl (1.0 mM). The surface charge of zeolite nanoparticles, Q, was calculated using the following equation:

$$Q = \frac{\sigma \times S_{BET}}{\text{Si/Al ratio}} \quad (2)$$

where, σ is the surface charge density, S_{BET} is the specific surface area, and Si/Al ratio is the silicon to aluminum ratio of the zeolite nanoparticles.

The porosity of zeolite nanoparticles were measured *via* adsorption and desorption of nitrogen using micrometrics ASAP 2010 volumetric adsorption analyzer. Samples were degassed at 250 °C under vacuum overnight prior to the measurement. The external surface area and micropore volume were estimated by alpha-plot method using Silica-1000 (22.1 m^2 g^{-1}) as a reference.

Collection of plasma. Informed consent was obtained from all subjects and this was approved by the Medical Ethical Committee of the Academic Medical Center Amsterdam under number W11_084/#11.17.864. The methods were carried out in accordance with the approved international guidelines. Blood was collected from healthy volunteers in tubes containing sodium citrate ($Na_3C_6H_5O_7$, Becton Dickson & Co., The Netherlands) as anticoagulant. Thereafter, the blood was centrifuged at 1500 × g for 20 min at 4 °C to collect plasma and subsequently all plasma samples were pooled and stored at −80 °C for further analysis.

Semi-quantitative assessment of each protein presents on corona zeolite nanoparticles. A semi-quantitative assessment of the protein amounts was conducted through the application of the spectral counting (SpC), based on the following equation[12,25]:

$$\text{NpSpC}_k = \left(\frac{\text{SpC}/(M_W)_k}{\sum_{i=1}^{n} \text{SpC}/(M_W)_i}\right) \times 100 \quad (3)$$

where $NpSpC_k$ is the normalized percentage of the spectral count for protein k, SpC is the spectral count identified, and M_w is the molecular weight (kDa) of protein k. The SpC of each identified protein was normalized to the protein mass and expressed as the relative quantity of protein. This correction is based on the protein size and evaluates the real contribution of each protein present in the corona of zeolite nanoparticles.

In order to identify the proteins with high affinity towards EMT- and FAU-zeolite nanoparticles, different concentrations of zeolite nanoparticles (4 and 12 wt%) were incubated for 60 min with different human plasma concentrations (10 and 100%). For comparison, two blank samples were applied: (1) Milli-Q water containing 1% formic acid, and (2) 100 μL nanoparticles were incubated with Milli-Q water containing 1% formic acid. After the incubations, all samples were centrifuged three times (24000 × g for 30 min) to remove the free plasma. Subsequently, all samples were subjected to tryptic digestion (trypsin: 100 ng/sample) at 37 °C for 24 h. Then the samples were centrifuged at 24000 × g for 60 min. The peptides were collected, and the zeolite nanoparticles were again re-suspended in 20 μL Milli-Q water containing 2% formic acid (three times vortexed during 45 min incubation and centrifuged at 24000 × g for 30 min). Finally, the peptides were collected and added to the first elution. All samples were then reduced with 1% dithiothreitol to break disulfide bridges. Finally, 2 μL of each sample-derived peptides fraction was injected into nLC-MS/MS (LTQ-ORBITRAP-XL). For each sample, two or three experiments were performed, measured by nLC-MS/MS to ensure high accuracy in the analysis.

The peptides were analyzed by nLC-MS/MS on an Ultimate 3000 system (Dionex, Amsterdam, The Netherlands) interfaced online with a LTQ Orbitrap XL mass spectrometer (Thermo Fisher Scientific, San Jose, CA). Re-dissolved peptides were loaded onto a trapping microcolumn (5 mm × 300 μm i.d.) packed with C18 PepMAP100 particles (5 μm, Dionex) in 0.1% formic acid at a flow rate of 20 μL min^{-1}. Upon loading and washing, the peptides were back flush eluted onto a nano-column (15 cm × 75 μm i.d.) packed with C18 PepMAP100 particles (3 μm, Dionex). The following mobile phase gradient was executed at a flow rate of 300 nL min^{-1}: 5–50% of solvent B in 93 min; 50–80% B in 5 min; 80% B for 10 min, and back to 5% B in 5 min. Solvent A was 100:0 H_2O–acetonitrile (v/v) with 0.1% formic acid, and solvent B was 10:90 H_2O–acetonitrile (v/v) with 0.1% formic acid. Peptides were infused in the mass spectrometer *via* a dynamic nano-spray probe (Thermo Electron Corp.) with a stainless steel emitter (Proxeon, Odense, DK). The typical spray voltage was 1.6 kV with no sheath and auxiliary gas flow; the ion transfer tube temperature was 200 °C. The mass spectrometer was operated in data-dependent mode.

Automated gain control (AGC) was set to 5×10^5 charges and 1×10^4 charges for MS/MS at the linear ion trap analyzer. The Data Dependent Acquisition (DDA) cycle consisted of the survey scan within m/z 300–1300 at the orbitrap analyzer with target mass resolution of 60000 (full width half maximum at m/z 400) followed by MS/MS fragmentation of the five most intense precursor ions under the relative collision energy of 35% in the linear trap. Singly charged ions were excluded from MS/MS experiments, and m/z of fragmented precursor ions were dynamically excluded for 90 s. The ion selection threshold for triggering MS/MS experiments was set to 500 counts. An activation parameter, q, of 0.25 and an activation time of 30 ms were applied.

PEAKS DB[45] (version 6.1) was applied to analyze the spectra/sample generated by nLC-MS/MS to identify proteins that bind to the layer (corona) of EMT- and FAU-zeolite nanoparticles. The total spectra per protein were determined by PEAKS DB to calculate the $NpSpC_k$ values. The structure of APOC-III and fibrinogen were drawn with PyMOL[46].

Effect of EMT- and FAU-zeolite on coagulation: prothrombin time (PT). To measure the time that is needed to clot the plasma portion of blood, prothrombin test (PT) was performed in pooled plasma with and without EMT- and FAU-zeolite nanoparticles in a KC-10 coagulometer. Three concentrations of EMT- and FAU-zeolite nanoparticles (0, 0.1 and 0.4%) were incubated with 100% pooled plasma derived from healthy volunteers for 30 min at room temperature and vortexed very gentle intermittently. Thereafter, prothrombin reagent was 10 times diluted; it contains a tissue factor and Ca^{2+} providing calcium ions supplement in the solution kept at 37 °C. From this reagent, 100 μL was added to each sample to start the reaction. The time between the addition of the thrombin and the clot formation is recorded as the thrombin clotting time (Sec).

References

1. Valtchev, V. & Tosheva, L. Porous Nanosized Particles: Preparation, Properties, and Applications. *Chem. Rev.* **113,** 6734–6760 (2013).
2. Mintova, S., Gilson, J.-P. & Valtchev, V. Advances in nanosized zeolites. *Nanoscale* **5,** 6693–6703 (2013).
3. Wu, J. *et al.* Protein adsorption onto nanozeolite: effect of micropore openings. *J. Colloid Interf. Sci.* **406,** 130–138 (2013).
4. Zhang, Y. *et al.* Zeolite/polymer composite hollow microspheres containing antibiotics and the *in vitro* drug release. *Journal of biomaterials science. Polymer edition* **22,** 809–822 (2011).
5. Young, S. W. *et al.* Gadolinium zeolite as an oral contrast agent for magnetic resonance imaging. *Journal of magnetic resonance imaging: J. Magn. Reson. Imaging* **5,** 499–508 (1995).
6. Flores-López, N. S. *et al.* Synthesis and properties of crystalline silver nanoparticles supported in natural zeolite chabazite. *J. Mol. Struct.* **1028,** 110–115 (2012).
7. Tavolaro, A., Riccio, I. I. & Tavolaro, P. Hydrothermal synthesis of zeolite composite membranes and crystals as potential vectors for drug-delivering biomaterials. *Micropor. Mesopor. Mater.* **167,** 62–70 (2013).
8. Yu, T. *et al.* Controlled nanozeolite-assembled electrode: remarkable enzyme-immobilization ability and high sensitivity as biosensor. *Chemistry* **12,** 1137–1143 (2006).
9. Ji, J. *et al.* Enhanced protein digestion through the confinement of nanozeolite-assembled microchip reactors. *Anal. Chem.* **80,** 2457–2463 (2008).
10. Hu, Y.-Y., Zhang, Y.-H., Ren, N. & Tang, Y. Crystal Plane- and Size-Dependent Protein Adsorption on Nanozeolite. *J. Phys. Chem. C* **113,** 18040–18046 (2009).
11. Baerlocher, C., McCusker, L. & Olson, D. *Atlas of zeolite framework types*. Elsevier Science B.V., 2007).
12. Laurent, S. *et al.* Corona protein composition and cytotoxicity evaluation of ultra-small zeolites synthesized from template free precursor suspensions. *Toxicol. Res.* **2,** 270–279 (2013).
13. Rezaee, F., Maas, a., Verheijen, J. H. & Koopman, J. Increased hepatic fibrinogen Bbeta-gene transcription is not enough to increase plasma fibrinogen levels. A transgenic mouse study. *Thromb. Haemostasis* **85,** 1025–1030 (2001).
14. Rezaee, F. *et al.* Overexpression of fibrinogen in ApoE*3-Leiden transgenic mice does not influence the progression of diet-induced atherosclerosis. *Thromb. Haemostasis* **88,** 329–334 (2002).
15. Gulledge, A. A., Rezaee, F., Verheijen, J. H. & Lord, S. T. A Novel Transgenic Mouse Model of Hyperfibrinogenemia. *Thromb. Haemostasis* **86,** 511–516 (2001).
16. Farrell, D., Mulvihill, E. & Huang, S. Recombinant human fibrinogen and sulfation of the gamma' chain. *Biochem.* **30,** 9414–9420 (1991).
17. Wolfenstein-Todel, C. & Mosesson, M. W. Human plasma fibrinogen heterogeneity: evidence for an extended carboxyl-terminal sequence in a normal gamma chain variant (gamma'). *P. Natl. Acad. Sci. USA* **77,** 5069–5073 (1980).
18. Redman, C. Fibrinogen Assembly and Secretion. ROLE OF INTRACHAIN DISULFIDE LOOPS. *J. Biol. Chem.* **271,** 30083–30088 (1996).
19. Meijer, K. *et al.* Human primary adipocytes exhibit immune cell function: adipocytes prime inflammation independent of macrophages. *PloS one* **6,** e17154 (2011).
20. Segrest, J. P. *et al.* The amphipathic helix in the exchangeable apolipoproteins: a review of secondary structure and function. *J. Lipid Res.* **33,** 141–166 (1992).
21. Zdunek, J. *et al.* Global structure and dynamics of human apolipoprotein CII in complex with micelles: evidence for increased mobility of the helix involved in the activation of lipoprotein lipase. *Biochem.* **42,** 1872–1889 (2003).
22. Lins, L. *et al.* Lipid-interacting properties of the N-terminal domain of human apolipoprotein C-III. *Protein Eng.* **15,** 513–520 (2002).
23. Vaz, W. L., Jacobson, K., Wu, E. S. & Derzko, Z. Lateral mobility of an amphipathic apolipoprotein, ApoC-III, bound to phosphatidylcholine bilayers with and without cholesterol. *Proceedings of the National Academy of Sciences of the United States of America* **76,** 5645–5649 (1979).
24. Assmann, G. & Brewer, H. B. A molecular model of high density lipoproteins. *P. Natl. Acad. Sci. USA* **71,** 1534–1538 (1974).
25. Monopoli, M. P. *et al.* Physical-chemical aspects of protein corona: relevance to *in vitro* and *in vivo* biological impacts of nanoparticles. *J. Am. Chem. Soc.* **133,** 2525–2534 (2011).
26. Walczyk, D., Bombelli, F. B., Monopoli, M. P., Lynch, I. & Dawson, K. A. What the cell "sees" in bionanoscience. *J. Am. Chem. Soc.* **132,** 5761–5768 (2010).

27. Mahmoudi, M. *et al.* Crucial role of the protein corona for the specific targeting of nanoparticles.*Nanomedicine* **10,** 215–226 (2015).
28. Behzadi, S. *et al.* Protein corona change the drug release profile of nanocarriers: The "overlooked" factor at the nanobio interface. *Colloids Surf. B Biointerfaces* **123,** 143–149 (2014).
29. Saꞗulkhu, U., Mahmoudi, M., Maurizi, L., Salaklang, J. & Hofmann, H. Protein Corona Composition of Superparamagnetic Iron Oxide Nanoparticleswith Various Physico-Chemical Properties and Coatings. *Sci. Rep.* **4,** 5020 (2014).
30. Hajipour, M. J., Laurent, S., Aghaie, A., Rezaee, F. & Mahmoudi, M. Personalized protein coronas: a "key" factor at the nanobiointerface. *Biomater. Sci.* **4,** 1210–1221 (2014).
31. Kollman, J. M., Pandi, L., Sawaya, M. R., Riley, M. & Doolittle, R. F. Crystal structure of human fibrinogen. *Biochem.* **48,** 3877–3886 (2009).
32. Marsh, J. J. *et al.* Structural insights into fibrinogen dynamics using amide hydrogen/deuterium exchange mass spectrometry. *Biochem.* **52,** 5491–5502 (2013).
33. Adamczyk, Z. *et al.* Fibrinogen conformations and charge in electrolyte solutions derived from DLS and dynamic viscosity measurements. *J. Colloid Interf. Sci.* **385,** 244–257 (2012).
34. Lousinian, S., Missopolinou, D. & Panayiotou, C. Fibrinogen adsorption on zinc oxide nanoparticles: a Micro-Differential Scanning Calorimetry analysis. *J. Colloid Interf. Sci.* **395,** 294–299 (2013).
35. Ng, E.-P., Chateigner, D., Bein, T., Valtchev, V. & Mintova, S. Capturing ultrasmall EMT zeolite from template-free systems. *Science* **335,** 70–73 (2012).
36. Pérez-Ramírez, J. Zeolite nanosystems: Imagination has no limits. *Nat. Chem.* **4,** 250–251 (2012).
37. Drechsler, A. & Grundke, K. The influence of electrolyte ions on the interaction forces between polystyrene surfaces. *Colloid. Surface A* **264,** 157–165 (2005).
38. Rezaee, F., Casetta, B., Levels, J. H. M., Speijer, D. & Meijers, J. C. M. Proteomic analysis of high-density lipoprotein. *Proteomics* **6,** 721–730 (2006).
39. Queiroz, K. C. S. *et al.* Human plasma very low density lipoprotein carries Indian hedgehog. *J. Proteome Res.* **9,** 6052–6059 (2010).
40. Sharifi, S. *et al.* Superparamagnetic iron oxide nanoparticles alter expression of obesity and T2D-associated risk genes in human adipocytes. *Sci. Rep.* **3,** 2173 (2013).
41. Klammt, S. *et al.* Albumin-binding function is reduced in patients with decompensated cirrhosis and correlates inversely with severity of liver disease assessed by model for end-stage liver disease. *Eur. J. Gastroenterol. Hepatol.* **19,** 257–263 (2007).
42. Gangabadage, C. S. *et al.* Structure and dynamics of human apolipoprotein CIII. *J. Biol. Chem.* **283,** 17416–17427 (2008).
43. Awala, H. *et al.* Template-free nanosized faujasite-type zeolites. *Nat. Mater.* **14,** 447–551 (2015).
44. Shan, X. *et al.* Measuring surface charge density and particle height using surface plasmon resonance technique. *Anal. Chem.* **82,** 234–240 (2010).
45. Zhang, J. *et al.* PEAKS DB: de novo sequencing assisted database search for sensitive and accurate peptide identification. *Mol. Cel. Proteomics* **11,** M111. 010587 (2012).
46. DeLano, W. L. The PyMOL Molecular Graphics System. *Schrödinger LLC wwwpymolorg* (Version **1.7.4.):** http://www.pymol.org (2002).

Author Contributions

M.R. and F.R. wrote the paper. F.R. conceived, designed and supervised the study. All authors (K.B., E.P.N., M.V., H.A.A., S.M., M.D., F.B., M.D.V., M.M.Z., M.P.P., M.M. and F.R.) involved in the experiments and generation of data as well as edition of the manuscript.

Additional Information

Supplementary information accompanies this paper at http://www.nature.com/srep

Competing financial interests: The financial support from the Region of Lower Normandy, the Zeoxy project is acknowledged for financial support. The financial support from Erasmus Medical Center, Rotterdam, The Netherlands.

How to cite this article: Rahimi, M. *et al.* Zeolite Nanoparticles for Selective Sorption of Plasma Proteins. *Sci. Rep.* **5**, 17259; doi: 10.1038/srep17259 (2015).